ESTIMATING RURAL ROOFTOP SOLAR POTENTIAL USING SEMANTIC SEGMENTATION AND MULTI-SOURCE DATA

Anonymous authors
Paper under double-blind review

ABSTRACT

Solar energy is a clean and renewable resource, and the low-rise, unobstructed rural buildings of northern China provide ideal conditions for photovoltaic (PV) installation compared to shaded, high-density urban areas. Yet, progress in assessing rural solar potential is limited by the absence of accurate 3D building data. This study proposes a rapid estimation approach integrating deep learning, parametric modeling, and GPU-accelerated simulation. Convolutional neural networks (CNNs) extract building footprints from satellite imagery, which are then processed in Grasshopper to generate refined vector outlines. Combined with digital surface model (DSM) data, these outlines produce precise 3D village models. Using Vitality 2.0 for GPU-based solar simulation, the method was applied to 31 villages in Tianjin, generating parametric 3D models and estimating their solar potential. Results show that low building heights and minimal mutual shading make photovoltaic capacity scale with roof area—larger villages have greater generation potential. Moreover, villages with metal roofs exhibit higher conversion efficiency and shorter cost-recovery periods than those with concrete or ceramic-tile roofs, due to better heat dissipation. Overall, the workflow offers a practical and efficient solution for estimating rural solar potential in data-scarce regions to guide renewable energy planning and investment.

1 INTRODUCTION

In recent decades, building roofs have been extensively studied in fields such as sustainable rural development, building energy simulation, and rural planning and design(Biljecki et al., 2015; Nouvel et al., 2017; Chen et al., 2020). With urbanization in the digital era, the demand for reliable information on roofs has grown significantly(Biljecki et al., 2016; Hu et al., 2021). Rapid acquisition of accurate roof information is crucial for assessing urban and rural development trends. These trends are instrumental in formulating development strategies and protecting urban and rural ecosystems. Particularly in the context of solar energy, China's vast rural areas, characterized by older buildings with high energy consumption, have led to the promotion of **photovoltaic (PV)** power generation in rural regions to conserve energy. Monocrystalline, polycrystalline, and amorphous-silicon PV panels are typically installed on roofs; consequently, roof scale and type largely determine rural PV potential. However, the lack of complete and detailed **three-dimensional (3D)** information on rural buildings in China hinders researchers from effectively estimating the potential for rural PV power generation.

Nevertheless, due to resource constraints, many developing countries lack data on roof areas, especially in rural regions of China. Therefore, there is an urgent need for cost-effective methods to generate reliable data on building roof areas. The automatic extraction of roof area data is gaining popularity across various fields, with research involving diverse data sources. 3D spatial data, such as **Digital Surface Models** (DSM) and **Light Detection and Ranging** (LiDAR), are used for reconstructing buildings, including roof area representation and geometric modeling(Chen et al., 2017a; Huang et al., 2019). However, the cost of acquiring 3D spatial data and con-structing related 3D models is high, particularly on an urban or rural scale. Yet, traditional image processing techniques involve complex empirical rules and threshold settings, presenting limitations when applied to large-scale high-resolution remote sensing images(Ye et al., 2019).

In recent years, deep learning methods have been employed for efficient feature learning and urban in-formation acquisition(Chen et al., 2018). Indeed, image semantic segmentation methods based on deep learning have been applied to extract roof data(Li et al., 2021). On the other hand, current deep learning methods for roof extraction primarily focus on plane recognition, lacking the acquisition of building height information, which prevents researchers from conducting urban 3D reconstruction through a single roof extraction method. This study will generate rural building models based on the CNBH-10m dataset and the plan of each rural building(Wu et al., 2023).

This study will use a new parametric method combined with deep learning-based building roof extraction for village building reconstruction and roof type classification. Finally, the study will conduct PV simulations based on the reconstructed village models and provide strategies for assessing the potential of PV power generation in villages through correlation analysis between the village's morphological indicators and simulation values.

2 METHODOLOGY

This study will be divided into the following steps to estimate the PV power generation potential of villages:1. Preparation of multi-source datasets; 2. Roof information extraction; 3. Generation of 3D village models; 4. Estimation of village PV power generation potential; 5. Analysis of village PV power generation potential. In the first step, the study will extract **satellite images (SI)** of villages and download the CNBH-10 building height dataset. In the second step, the SI images will be input into a pretrained deep learning model to extract roof information and generate **roof semantic segmentation images (RI)**. In the third step, the RI images and CNBH-10 data will be input into the parametric design software Grasshopper, and multi-source data integration will be performed using the Grasshopper plugin Bitmap+ to ultimately generate 3D village models. In the fourth step, the obtained 3D village models will be input into Grasshopper, and the PV power generation potential of village roofs will be calculated using the Grasshopper plugin Vitality 2.0. In the fifth step, the study will conduct a correlation analysis based on the village PV power generation output, village morphological indicators, and roof classification results, summarizing a reasonable methodology for researchers to evaluate the PV power generation potential of villages.

2.1 MULTI-SOURCE DATASET PREPARATION

2.1.1 RURAL AREA DELINEATION

This study will primarily focus on the rural areas of the Tianjin Grand Canal region within the Beijing-Tianjin-Hebei area. A total of 31 rural areas were selected for the study. On the other hand, the study found that the selected villages exhibit certain patterns in their planar layouts. The study will classify these villages based on morphological indicators.

2.1.2 SATELLITE IMAGE PREPARATION

The study acquires rural SI through the Jilin-1 Satellites, which represent China's first independently developed commercial high-resolution remote sensing satellites(Zheng et al., 2018).

2.1.3 CNBH-10M DATASET

The study adopts the CNBH-10m dataset proposed by Wu. as the building height information data for rural villages(Wu et al., 2023). Wu et al. utilized **Ground Range Detected (GRD)** scenes from Sentinel-1 to estimate urban building heights. These data are derived from the dual-polarization C-band **Synthetic Aperture Radar (SAR)** instrument, which offers a resolution of 10 meters and a short revisit time (6-12 days). To evaluate the accuracy of the building height estimation, the study calculates several metrics, including the correlation coefficient, **root mean square error (RMSE)**, and **mean absolute error (MAE)**. The results show that the **Weighted Least Squares (WLS)** regression model achieves an average R value of 0.7, an RMSE of 6.2 meters, and an MAE of 5.2 meters, indicating that the model has strong generalizability across different regions.

2.2 Deep Learning-Based Roof Information Extraction Model

This study employs the building roof information extraction method developed by Zhang et al. (Zhang et al., 2022). Zhang utilized the **DeepLabV3+ model**(Chen et al., 2017b) and **Google Earth Studio (GES)** images to extract building roof information from satellite data. The methodology primarily leverages high-resolution remote sensing images from Google Earth as the primary data source, incorporating the **30-meter global land cover dataset (FROMGLC30)** for spatial stratified sampling.

DeepLabV3+, an open-source semantic-segmentation model from Google, is well suited to GES imagery where roof size and shape vary and weather can degrade image quality. Its multi-scale feature perception improves recognition across diverse roof types, while the encoder–decoder pro-duces fixed-resolution out-puts that mitigate edge blurring in rooftop extraction. Following Zhang et al., we use their final model—fine-tuned on COCO with Adam and a learning-rate annealing schedule—to segment rural SI.

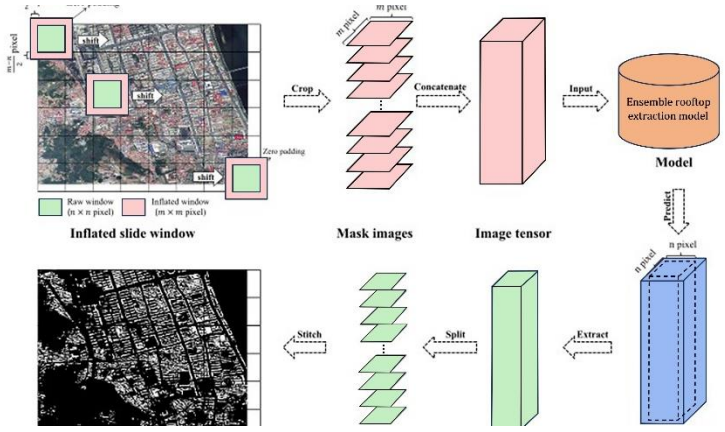

Fig. 1 Conceptual diagram of Zhang's roof extraction method

2.3 3D Village Model Generation

The study inputs SI and RI obtained from semantic segmentation into the Grasshopper(Sung & Jeong, 2022) parametric platform. The SI images serve as the baseline for visualization, while the **Bitmap+ plugin** is used to extract roof contour lines from the RI images. After obtaining the roof contour lines, the study employs the minimum bounding rectangle method to generate the smallest rectangular bounding box for each closed contour line. The rectangular boxes are then divided into a 3×3 grid, and grids that do not inter-sect with the initial contour lines are removed. This process results in **rationalized contour lines (BL)** that closely approximate the original roof shapes.

Next, the study reads the CNBH-10m dataset in TIFF format for the target villages using **Global Mapper** and exports the elevation data using the **Arc ASCII Grid** method. The elevation data is then imported into Grasshopper through the **Docofossor plugin**, where it is converted into an elevation grid. For each BL, the study extracts the center points of the 3×3 grids and identifies the nearest elevation grid point along the Z-axis to determine the elevation information of the center points. Based on the average elevation values of all grid points within each contour line, the study determines the elevation information for the contour lines and generates **3D building blocks (3DM)**.

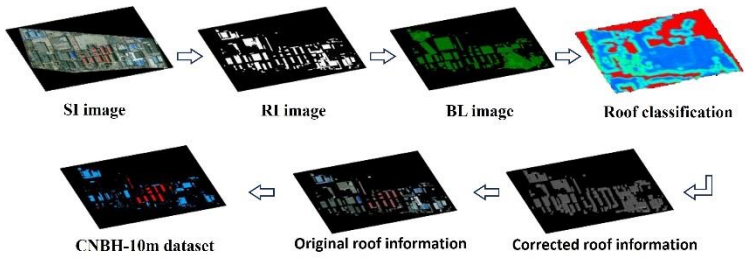

Fig. 2 The workflow for generating parametric 3D models of villages

This study uses a parametric approach to classify building roofs. The process involves extracting the **original color (OC)** corresponding to each 3×3 grid center point within BL from the village SI. The RGB channels of OC, which range from 0 to 255, are each divided into three equal parts, resulting in 27 distinct color ranges. The colors of each grid are then classified into one of these 27 color ranges based on their RGB values .

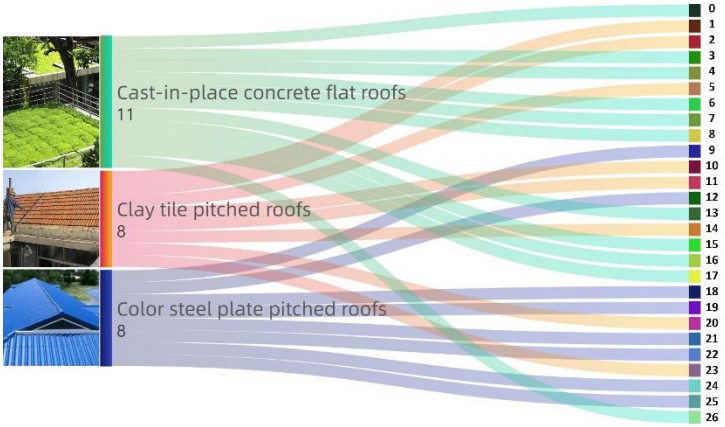

Fig. 3 The conceptual diagram of the classification of 27 colors.

In China, rural roof materials are primarily divided into traditional and modern materials. With rural development, some materials have been phased out, and the following three types are now widely adopted:1. Concrete flat roofs;2. Clay tile pitched roofs;3. Color steel plate pitched roofs. Since concrete flat roofs are suitable for drying grain or planting vegetation, some **concrete roofs (CR)** appear yellow or green. The study further categorizes the 27 color ranges into three types:1. CR;2. Clay tile pitched roofs (TR);3. Color steel plate pitched roofs (MR). Given that clay tile and color steel plate roofs are predominantly pitched, the study will reconstruct 3D models for these types of roofs.

2.4 Calculation method for the potential of photovoltaic power generation

This study employs a simulation method based on the Perez diffuse sky model(Driesse et al., 2024) for solar radiation computation and calculates PV power generation using the corresponding formulas.

The complexity of solar radiation computation in a village environment is determined by the distribution characteristics of solar radiation. Firstly, the study requires support from **Typical Meteorological Year (TMY)** data. In the solar radiation component of the TMY data, only the direct and diffuse radiation on a horizontal surface is provided. Therefore, based on the existing radiation data, it is necessary to calculate the reflected radiation on each building surface. The total radiation on a building surface should consist of three components: direct radiation, diffuse radiation, and reflected radiation:

$$G_i = G_{bi} + G_{di} + G_{ri}$$

where $G_i$represents the total solar radiation on the building surface, G_{bi} denotes the direct solar radiation on the building surface, $G_{di}$is the diffuse solar radiation on the building surface, and G_{ri} signifies the reflected solar radiation on the building surface.

Since the building units are treated as cubes in the 3D rural model construction, in addition to calculating the solar radiation on the roof (horizontal surface), it is also necessary to convert the horizontal radiation data from TMY file into solar radiation for vertical surfaces with different orientations and a 90° tilt. For the direct solar radiation on an inclined surface (with a tilt angle of i), the calculation formula is as follows:

$$G_{bi} = G_b * \frac{\cos\theta_i}{\sin\alpha_s}$$

where $G_b$represents the total direct solar radiation on the horizontal surface, θ_i is the surface tilt angle, and $\alpha_s$denotes the solar altitude angle. The reflected radiation on the inclined surface can be calculated using the following formula:

$$G_{ri} = （G_{bi} + G_{di}） * \rho * \frac{1 - \cos\beta}{2}$$

The calculation of diffuse radiation on an inclined surface is relatively complex. According to the Reindl model(Wan-Ben et al., 2023)(19), the calculation formula is as follows:

$$G_{di} = G_d \left[\left(1 - \frac{G_b}{G_o}\right) \left(1 + \sqrt{\frac{G_b}{G}} \sin\left(\frac{\beta}{2}\right)\right) \frac{1 + \cos\beta}{2} + \frac{G_b}{G_o} R_b \right]$$

where G_d represents the total diffuse solar radiation on the horizontal surface, and G_o denotes the hourly solar radiation on the horizontal surface.

The method can calculate solar radiation on building surfaces with different orientations and tilt angles based on horizontal solar radiation data from TMY, offering a certain level of accuracy. The study uses the Perez diffuse sky model(Woojae et al., 2022), which is well-suited for calculating solar radiation on building surfaces in rural environments.

Due to differences in PV cell materials, the photoelectric conversion efficiency of PV modules varies, leading to different thresholds for different modules. Additionally, although there are many types of PV modules available on the market, their prices and efficiencies differ significantly. Selecting the appropriate PV modules is therefore a critical factor in ensuring the rationality of PV power generation potential assessments. Specifically, this study considers the PV power generation potential of different roof types, as research has shown that TR and MR require higher installation costs, which must be considered in the study.

The study selects monocrystalline silicon PV panels primarily due to their high efficiency. Since the PV power generation potential assessment is based on the available area for calculating power generation and the system's installed capacity is unknown, the study adopts the module area method to estimate the power generation of the PV system. This method is used to calculate the potential power generation of a PV system by evaluating the effective area available for installing PV modules. The formula is as follows:

$$E_p = H_A * A_{pv} * \eta_{pv} * PR$$

where $\mathbf{E_p}$ represents the annual power generation of the PV system in kWh; $\mathbf{H_A}$ denotes the annual cumulative solar radiation in kWh; $\mathbf{A_{pv}}$ is the area of the PV modules (available surface area of the building) in m²; $\boldsymbol{\eta_{pv}}$ is the efficiency of the PV modules in %; and **PR** is the performance ratio in %. Kumar et al. (Yu et al., 2022) conducted a statistical analysis of the performance of 23 PV systems worldwide. According to their findings, the **PR** values of current PV systems generally range between 80% and 90%, with some systems even exceeding 90%. In this study, the PR value is set to 90%.

Although the PV power generation can provide a direct assessment of the PV potential in villages, it is also necessary to consider the varying installation costs of PV panels on different roof types and the impact of roof heat dissipation on PV panel performance. To evaluate the PV potential more comprehensively, the study calculates the expected return on investment of PV panels. By comparing the installation costs of PV panels with their annual power generation revenue, a key indicator—the expected payback period—can be determined. This indicator helps identify the most suitable PV system for traditional protected village areas. The calculation formula is as follows:

$$N = \frac{（C_I + C_s）* A_{PV}}{C_E * E_p}$$

where **N** represents the expected payback period in years; $\mathbf{C_I}$ denotes the cost of PV panels in RMB/m²; $\boldsymbol{C_s}$is the installation cost of PV panels in RMB/m²; A_{pv} is the area of PV modules (roof surface area) in m²; $\mathbf{C_E}$is the electricity price in RMB/kWh, with the upper limit of the electricity price in market transactions being 1.2 times the benchmark price, i.e., 0.49932 RMB/kWh; and E_p is the annual power generation of the PV system in kWh.

This study uses monocrystalline silicon PV panels as the ideal material for PV power generation. Through investigation(Zhi et al., 2022), it was found that the initial solar radiation threshold for monocrystalline silicon PV panels is 100 W/m². Due to better heat dissipation on MR, the $\eta_{pv}$of PV modules installed on such roofs is higher.

Roof type	Cost of PV panels	Cost of auxiliary materials	Reinforcement cost	Labor Cost	Total Cost	η_{pv}
CR	1500 RMB/ m²	625 RMB/ m²	0 RMB/ m²	375 RMB/ m²	2500 RMB/ m²	20%
TR	1500 RMB/ m²	625 RMB/ m²	650 RMB/ m²	375 RMB/ m²	3150 RMB/ m²	20%
MR	1500 RMB/ m²	625 RMB/ m²	300 RMB/ m²	375 RMB/ m²	2800 RMB/ m²	24%

Table 1 Three rooftop solar panel settings

The study reveals that the installation costs vary significantly depending on the roof type, primarily due to whether reinforcement is required for mounting PV panels(Qi et al., 2022). Other labor and auxiliary material costs will be uniformly set in this study. Regarding reinforcement costs:1. Concrete flat roofs generally do not require reinforcement, resulting in lower costs;2. Clay tile pitched roofs require additional wooden beams and brackets for reinforcement, leading to higher costs;3. MR necessitates the use of clamps and wind-resistant reinforcement, also resulting in higher costs.

2.5 Village PV Potential Analysis Method

To provide researchers with a method for quickly estimating the PV power generation potential of villages and to offer design strategies related to PV potential, this study will analyze the correlation between village morphological indicators and PV potential indicators ($\mathbf{E_p}$and **N**). During the generation of 3D village models in Section 2.3, the study recorded the following morphological indicators:1. Village **total land area (TA)**;2. **Village building density (BAR)**;3. Village **floor area ratio (FAR)**;4. Average **building height (BH)** of the village； 5. The **orientation angle (OA)** is related to the south. Additionally, since the study considers different roof types, the following data were recorded:1. Proportion of CR (CR);2. Proportion of TR(TR);3. Proportion of MR(MR).

This research will establish a predictive model correlating morphological indicators with solar energy potential metrics through regression algorithms. Given the potential multicollinearity among morphological indicators, **Principal Component Analysis (PCA)** will be employed to identify and select significant components. The study will subsequently construct regression models for solar energy potential prediction using these selected components. To address multicollinearity challenges, the ridge regression algorithm - which incorporates L2 regularization - will be adopted for model development due to its demonstrated efficacy in handling correlated predictor variables.

3 Result

The study extracted roof information from SI of all 31 villages and generated parameterized 3D village models. Additionally, PV simulations were conducted on the generated 3D models. As shown in Figure 4, the study found significant variations in E_p among the villages. The highest-performing village can generate over 20,000,000 kWh/year, while the lowest-performing village generates less than 5,000,000 kWh/year, representing a difference of more than four times.

As illustrated in Figure 4, the study also observed considerable variation in N among the villages. The maximum Nvalue exceeds 25 years, while the minimum N value is less than 17 years. Furthermore, the study found that the trend in E_p does not align with the trend in N. This discrepancy indicates that the morphological differences among villages lead to varying power generation costs, resulting in inconsistent trends between the two indicators.

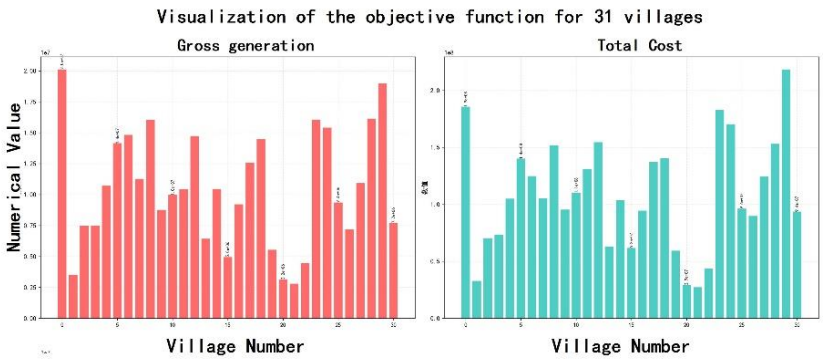

Fig. 4 The total annual rooftop solar power generation of 31 villages (left) and the expected payback period in years of 31 villages (right)

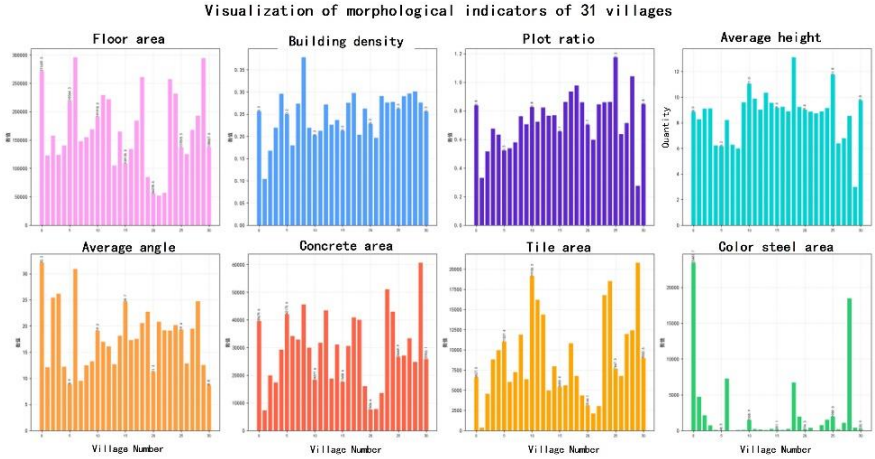

Fig. 5 The graph of 8 morphological indicators of 31 villages

As shown in Figure 5, the study obtained morphological indicators for the 31 villages. The analysis revealed that the BH in these villages does not exceed 15 meters, indicating that the villages primarily consist of low-rise buildings with minimal mutual shading issues. Additionally, the study found that BAR in these villages does not exceed 0.4, suggesting that the buildings are not densely distributed. On the other hand, the study observed that CR dominate the majority of the villages. In some villages, CR accounts for over 80% of the total roof area, while even in villages with the lowest proportion, CR still exceeds 40%. In contrast, MR generally occupies a smaller proportion, with only five villages having a color steel roof proportion exceeding 10%. This indicates that the target villages are predominantly residential, with buildings mainly used for housing, rather than industrial villages dominated by MR.

4 Analysis

4.1 Correlation Analysis

The study uses a correlation analysis between the morphological indicators of the villages, roof information, and PV power generation potential indicators (E_p and N). As shown in Figure 6, the results are presented as follows:

1. For **total power generation (E_total)**, **TA (Total Architecture)** shows a very strong positive correlation (r=0.88) with E_total, as more buildings provide larger available roof area for PV installation; **BAR (Building Area Ratio)** demonstrates a positive correlation (r=0.43) with E_total, since higher building coverage ratio corresponds to greater roof area.

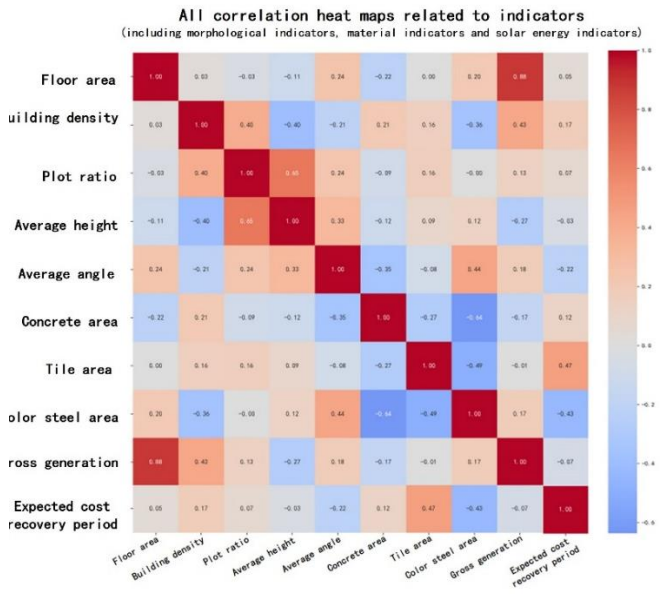

Fig. 6 Correlation visualization chart

2. Regarding **expected payback period (N)**, TR exhibits a positive correlation (r=0.47) with N, indicating that villages with more sloped roofs have longer cost recovery periods due to reduced suitable area for solar panel installation; MR shows a negative correlation (r=-0.43) with N, meaning villages with larger metal roof areas can recoup costs in shorter timeframes.
3. The study also identified strong correlations among certain morphological indicators: average building height shows a strong positive correlation with floor area ratio (r=0.65), while demonstrating a moderate negative correlation with building density (r=-0.40).

4.2 Principal Component Analysis

Prior to conducting regression analysis, the study examined multicollinearity among indicators through **Variance Inflation Factor (VIF)** analysis. As shown in Figure 7, with the exception of MR, TR, and OA indicators, all other indicators exhibited severe multicollinearity issues.

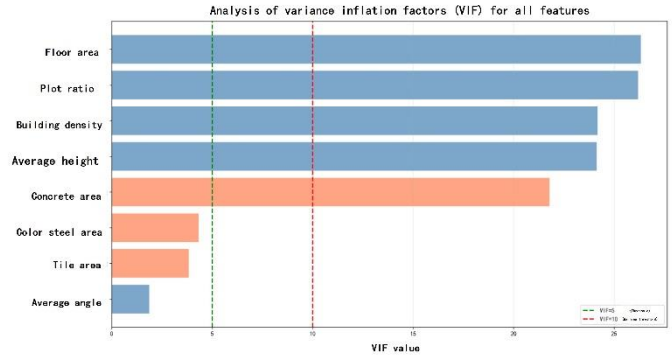

Fig.7 Visualization of Indicator VIF Analysis

If indicators with severe multicollinearity are used to establish a regression model, the variance of the estimated regression coefficients will significantly increase, making them sensitive to minor changes in sample data and resulting in unstable estimation outcomes. On the other hand, using indicators with high multicollinearity will reduce the interpretability of the regression model. Therefore, prior to constructing the regression model, the study employed PCA to screen for important indicators.

Since the study involves eight indicators, four principal components were set. Indicators with contributions exceeding 1.0 for these four principal components were selected for further analysis. As shown in Figure 8a, the study found that five indicators had cumulative contribution values exceeding 1.0 across the four principal components. These included building density, site area, CR, TR, and average height, all of which exhibited PCA weights greater than 1.5.

As shown in Figure 8b, the study conducted VIF analysis on the screened indicators. The results showed that all five indicators had VIF values below 2, indicating no significant multicollinearity among them.

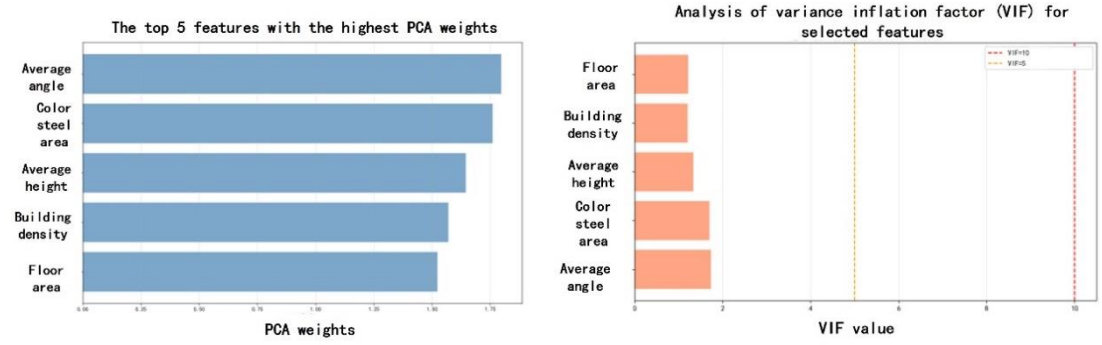

a b

Fig.8 Visualization of PCA Weight Analysis (a) | Visualization of VIF Analysis for Selected Indicators (b)

4.3 Ridge Regression Model

The study established ridge regression models for the five selected indicators relative to the objective functions. To compare the contribution values of each indicator to the ridge regression model, the data were normalized. To evaluate the performance of each model, the study assessed the models using four metrics: R^2, RMSE, MAE, and MAPE. Furthermore, to enhance the reliability and generalizability of the model evaluation, three-fold cross-validation was performed.

As shown in Figure 9, ridge regression models were developed for N and E_total, with the following findings:

For N (expected payback period), the ridge regression model achieved an R^2 value below 0.3. However, its RMSE (relative error < 9%), MAE (relative error < 8%), and MAPE (relative error < 8%) performances were acceptable. This indicates a nonlinear relationship between the indicators and N, which the regression model could not fully capture, leading to a low R^2 value, though the error remained within acceptable limits.

For total power generation (E_total), the ridge regression model achieved an R^2 value exceeding 0.95. Meanwhile, the relative errors of RMSE, MAE, and MAPE were all below 10%, indicating excellent model performance. The ridge regression formula (after normalization) for total power generation is as follows: E_total = -0.0111 + 0.4383 × Building Density + 0.8329 × Site Area - 0.1072 × Concrete Roof Ratio - 0.1027 × Tile Roof Ratio + 0.0049 × Average Height.

This formula reveals that building density and site area have significant impacts on the total solar power generation potential of village roofs.

To validate the rationality and generalizability of the ridge regression models, a three-fold cross-validation experiment was conducted. As shown in Figure 10, the results demonstrate:

For N, the cross-validation experiment showed an R^2 value below zero, while the relative errors of RMSE, MAE, and MAPE remained below 8%. This suggests that the ridge regression algorithm failed to learn the underlying patterns of N.
For E_total, the cross-validation experiment achieved an R^2 value above 0.80, with low relative errors in RMSE, MAE, and MAPE, confirming the robust performance of the ridge regression model.

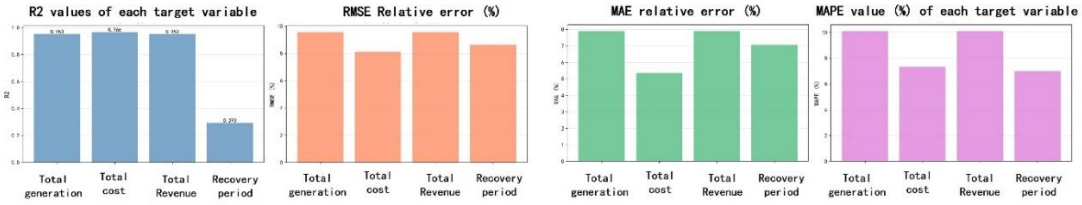

Fig.9 Visualization of Ridge Regression Model Performance for Solar Potential Indicators

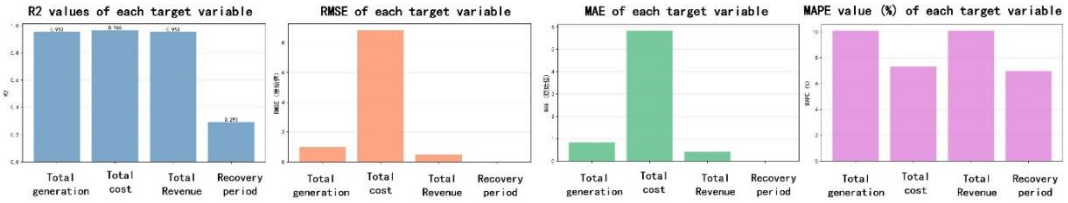

Fig.10 Visualization of Ridge Regression Model Performance

5 CONCLUSION & FUTURE RESEARCH

The study used deep learning models and multi-source data to generate 3D models of rural areas surrounding Tianjin. The study employed the deep learning model to extract roof information from SI. Subsequently, the study rationalized the roof contour lines using a parametric approach and integrated the CNBH-10m dataset to generate 3D village models. To more accurately assess the PV power generation potential of village roofs, the study applied different PV panel settings and cost assumptions based on roof types. Based on correlation analysis, the study found the following:

1. Since village buildings are generally low-rise, they do not suffer from mutual shading issues commonly seen in urban areas. Therefore, larger villages with more buildings tend to have higher PV power generation potential.
2. Based on correlation analysis, the study found that TR and MR exhibit certain correlations with N (expected payback period). The research reveals that villages with more sloped-roof buildings (higher TR values) have less available area for rooftop solar panel installation, resulting in larger N values. On the other hand, due to lower installation costs of solar panels on metal roofs, villages with more metal-roofed buildings (higher MR values) incur lower overall costs for solar panel installation, enabling them to recover costs within a shorter period.
3. Based on ridge regression modeling, the study identified that both village site area and building density among morphological indicators show strong correlations with village rooftop solar power generation capacity.

Despite these findings, the study has the following limitations:

1. The villages studied were selected randomly without considering different morphological types, which limits the generalizability of the conclusions.
2. The study focused on a limited number of villages, which restricts the ability to draw more comprehensive and valuable conclusions.
3. The study did not model the PV panels in detail, such as their installation angles or individual panel dimensions, which could affect the accuracy of the PV power generation potential assessment.
4. Since the study primarily focused on low-rise buildings, it could not analyze the impact of building height on rooftop PV power generation potential.

Future research will expand the scope of target villages and classify them based on morphological indicators. Additionally, the study will incorporate more detailed modeling of PV panels based on roof types and consider factors such as panel dimensions.

REFERENCES

Filip Biljecki, Gerard BM Heuvelink, Hugo Ledoux, and Jantien Stoter. Propagation of positional error in 3d gis: estimation of the solar irradiation of building roofs. *International Journal of Geographical Information Science*, 29(12):2269–2294, 2015.

Filip Biljecki, Ken Arroyo Ohori, Hugo Ledoux, Ravi Peters, and Jantien Stoter. Population estimation using a 3d city model: A multi-scale country-wide study in the netherlands. *PloS one*, 11(6): e0156808, 2016.

Dong Chen, Ruisheng Wang, and Jiju Peethambaran. Topologically aware building rooftop reconstruction from airborne laser scanning point clouds. *IEEE Transactions on Geoscience and Remote Sensing*, 55(12):7032–7052, 2017a.

Guanzhou Chen, Xiaodong Zhang, Qing Wang, Fan Dai, Yuanfu Gong, and Kun Zhu. Symmetrical dense-shortcut deep fully convolutional networks for semantic segmentation of very-high-resolution remote sensing images. *IEEE Journal of Selected Topics in Applied Earth Observations and Remote Sensing*, 11(5):1633–1644, 2018.

Liang-Chieh Chen, George Papandreou, Florian Schroff, and Hartwig Adam. Rethinking atrous convolution for semantic image segmentation. *arXiv preprint arXiv:1706.05587*, 2017b.

Yang Chen, Luliang Tang, Xue Yang, Muhammad Bilal, and Qingquan Li. Object-based multimodal convolution neural networks for building extraction using panchromatic and multispectral imagery. *Neurocomputing*, 386:136–146, 2020.

Anton Driesse, Adam R Jensen, and Richard Perez. A continuous form of the perez diffuse sky model for forward and reverse transposition. *Solar Energy*, 267:112093, 2024.

Qintao Hu, Liangli Zhen, Yao Mao, Xi Zhou, and Guozhong Zhou. Automated building extraction using satellite remote sensing imagery. *Automation in Construction*, 123:103509, 2021.

Jianfeng Huang, Xinchang Zhang, Qinchuan Xin, Ying Sun, and Pengcheng Zhang. Automatic building extraction from high-resolution aerial images and lidar data using gated residual refinement network. *ISPRS journal of photogrammetry and remote sensing*, 151:91–105, 2019.

Arash Kazemian, Hongxing Yang, and Changying Xiang. Assessing the effects of photovoltaic and solar thermal ratios on performance, cost, and emissions in combined solar configurations. *Applied Energy*, 384:125438, 2025.

Sandip Ravi Kumar, Francisco Gafaro, Andrew Daka, and Atul Raturi. Modelling and analysis of grid integration for high shares of solar pv in small isolated systems–a case of kiribati. *Renewable Energy*, 108:589–597, 2017.

Peiran Li, Haoran Zhang, Zhiling Guo, Suxing Lyu, Jinyu Chen, Wenjing Li, Xuan Song, Ryosuke Shibasaki, and Jinyue Yan. Understanding rooftop pv panel semantic segmentation of satellite and aerial images for better using machine learning. *Advances in applied energy*, 4:100057, 2021.

Romain Nouvel, Maryam Zirak, Volker Coors, and Ursula Eicker. The influence of data quality on urban heating demand modeling using 3d city models. *Computers, Environment and Urban Systems*, 64:68–80, 2017.

Nuno Ba´ıa Saraiva, Euge´nio Rodrigues, Ade´lio Rodrigues Gaspar, and Jose´ Joaquim Costa. Daylighting simulation of a heritage building by comparing matrix methods and solar models. *Solar Energy*, 224:685–696, 2021.

Woojae Sung and Yohan Jeong. Site planning automation of apartment complex through grid-based calculation in grasshopper. *Automation in construction*, 138:104216, 2022.

Wan-Ben Wu, Jun Ma, Ellen Banzhaf, Michael E Meadows, Zhao-Wu Yu, Feng-Xiang Guo, Dhritiraj Sengupta, Xing-Xing Cai, and Bin Zhao. A first chinese building height estimate at 10 m resolution (cnbh-10 m) using multi-source earth observations and machine learning. *Remote Sensing of Environment*, 291:113578, 2023.

Yu Ye, Daniel Richards, Yi Lu, Xiaoping Song, Yu Zhuang, Wei Zeng, and Teng Zhong. Measur- ing daily accessed street greenery: A human-scale approach for informing better urban planning

Zhixin Zhang, Zhen Qian, Teng Zhong, Min Chen, Kai Zhang, Yue Yang, Rui Zhu, Fan Zhang, Haoran Zhang, Fangzhuo Zhou, et al. Vectorized rooftop area data for 90 cities in china. *Scientific Data*, 9(1):66, 2022.

Qiming Zheng, Qihao Weng, Lingyan Huang, Ke Wang, Jinsong Deng, Ruowei Jiang, Ziran Ye, and Muye Gan. A new source of multi-spectral high spatial resolution night-time light imagery—jl1-3b. *Remote sensing of environment*, 215:300–312, 2018.